Astron. Astrophys. 177, 292–302 (1987)

ASTRONOMY AND ASTROPHYSICS

Acoustic tube waves in the solar atmosphere

I. Magnesium and calcium line emission with complete redistribution

P. Ulmschneider[1], **D. Muchmore**[1], **and W. Kalkofen**[2]

[1] Institut für Theoretische Astrophysik, Im Neuenheimer Feld 561, D-6900 Heidelberg, Federal Republic of Germany
[2] Harvard-Smithsonian Center for Astrophysics, 60 Garden Str., Cambridge MA 02138, USA

Received November 18, accepted December 19, 1986

Summary. The propagation of acoustic waves through vertical magnetic flux tubes in the solar atmosphere was computed with radiation damping by (non-LTE) emission from H^- and the Mg II k line. Waves of various amplitudes and periods were investigated in flux tubes with three different spreading rates characterized by the radius as a i) constant, ii) linear or iii) exponential function of height. The geometry of the flux tubes greatly influences the behaviour of the waves. Large wave amplitudes and intense postshock radiative relaxation zones are found in constant tubes while small amplitudes and weak radiation zones were found in exponential tubes. In all calculations following Mg II ionization, transition-layer-like rapid temperature rises formed and transient mass flows were initiated. In constant tubes the rapid temperature rises occurred at low heights while in exponential tubes these layers were found much higher. Waves with longer periods produced steep temperature rises at lower height and led to more mass motion. The heights of the rapid temperature rises did not depend much on the initial wave energy flux.

Key words: chromosphere – acoustic waves – flux tubes – Mg II lines

1. Introduction

In recent years it has become increasingly clear that acoustic-like waves reemerge as the leading candidate for the heating mechanism of stellar chromospheres. This is especially surprising since only a few years ago it was concluded from Mg II line observations obtained with the International Ultraviolet Explorer (IUE)-satellite (Basri and Linsky, 1979) that the acoustic heating theory cannot explain the chromospheric emission of stars. In particular the observation that stars with similar effective temperature $T_{\rm eff}$ and gravity g differ greatly in their chromospheric emission showed that the emission is strongly tied to the magnetic field. This fits quite well with the implication long recognized from solar observations that chromospheric emission is intimately correlated with the magnetic field.

The magnetic field appears on the solar surface in the form of highly concentrated flux tubes (Stenflo, 1978; Zwaan, 1978), suggesting magnetohydrodynamic (MHD) tube waves as a possible agent in chromospheric heating. Stein (1981) and Ulmschneider and Stein (1982) showed that in magnetic regions the slow-mode and Alfvén-mode MHD wave generations are greatly enhanced. In addition Herbold et al. (1985) showed that the slow-mode-like longitudinal MHD tube waves and acoustic tube waves are essentially identical in their propagation and heating properties. Thus, if the enhanced energy generation, the magnetic field geometry and the propagation along the field are taken into account the acoustic wave-like shock heating theory is once more a very likely candidate for the mechanism which produces stellar chromospheres. For a recent review of chromospheric heating theories see Ulmschneider (1986b).

The important differences compared with earlier acoustic wave computations (e.g. Ulmschneider et al., 1977, 1978; Schmitz et al., 1985) are that in the present work the magnetic flux tube geometry and radiation losses by metal lines are explicitly taken into account. The rate at which an individual flux tube spreads with height depends on the environment in which it finds itself, being faster for isolated tubes – such as perhaps in interior regions of supergranulation cells – and slower for tubes with nearby neighbours – such as those in active regions or at supergranulation boundaries. Since various types of spreading are possible, we investigate the acoustic wave propagation in tubes of different geometries.

A recent review of time-dependent MHD wave calculations in stellar atmospheres (Ulmschneider and Muchmore, 1986) describes the different types of radiation treatment possible in various regions of the atmosphere. In the photosphere the radiation losses may be computed assuming LTE. For the upper transition region and lower corona, radiation losses can be computed in the thin plasma approximation using a simple function of temperature and pressure. In the intermediate atmospheric region the chromosphere and lower transition layer, neither of these approximations is appropriate. Empirical models show that in the temperature minimum region and the low chromosphere the H^- continuum and the infrared CO molecular band are the most important radiation loss mechanisms (Vernazza et al., 1981; Ayres, 1981; Muchmore and Ulmschneider, 1985). At the middle chromosphere the radiation loss is mainly due to line emission from the h and k lines of Mg II as well as the H, K and infrared triplet lines of Ca II while in the upper chromosphere and lower transition layer the Lyman continuum and the Lyman lines of hydrogen are the most important emitters.

For all of these chromospheric line and continuum radiation loss mechanisms, departures from LTE are essential. This applies

Send offprint requests to: P. Ulmschneider

not only to the emitter at hand but also to the thermodynamic structure of the atmosphere. The emission by H^-, Mg and Ca for instance is directly proportional to the electron density, which in the chromosphere is strongly affected by departures from LTE in hydrogen and by the hydrogen ionization. The treatment of departures from LTE in H^- for time-dependent cases has been described by Schmitz et al. (1985).

The present work discusses the inclusion of time-dependent emission by the important lines of metallic ions in atmospheric wave calculations. To make the problem tractable rough approximations have to be made in the atomic model of these ions and in the transitions considered: we assume an atom with two bound levels. Hence the infrared triplet lines of Ca II can obviously not be described. Under this restriction, we present static calculations for both Mg II and Ca II. By comparison with the more detailed models of Vernazza et al. (1981), we justify the simplification used in our dynamic models that one line (Mg II) can be used to represent the total middle chromospheric emission. In Sect. 2 we discuss the selection of the flux tube models, the hydrodynamic method and describe our procedure for treating the Mg II and Ca II line emission. Section 3 gives a comparison with the solar model computations of Vernazza et al. Section 4 shows the results of our chromospheric wave calculations and Sect. 5 presents our conclusions.

2. Method of computation

We consider acoustic wave propagation in a series of rigid tubes whose cross-sections increase differently with height. These tubes are assumed to represent the various geometric shapes of solar magnetic flux tubes arising from different amounts of crowding experienced at the centers of supergranulation cells, in the network and in active regions. As shown by Herbold et al. (1985) acoustic wave propagation along rigid tubes closely approximates the propagation of longitudinal magnetohydrodynamic waves along thin magnetic tubes.

2.1. Initial flux tube models

To investigate the influence of the tube geometry on the propagation and radiative properties of the wave we have chosen three different types of flux tubes. The tubes are assumed to be oriented along a vertical axis and to spread horizontally in a plane non-magnetic density-stratified atmosphere as a result of pressure balance similar to Herbold et al. There are different possible choices for such an outside atmosphere. Muchmore and Ulmschneider (1985) have discussed various radiative equilibrium atmospheres which, depending on the solar region considered, may be dominated by a cold CO emitting layer. These CO layers however do not form if the effective temperature is higher than 5900 K or if significant acoustic heating occurs in the atmosphere.

As the turbulent solar convection zone will always produce some measure of acoustic energy and as the nonmagnetic regions lie above the relatively hot interiors of the granulation cells we assume that the non-magnetic region can be represented by a radiative equilibrium atmosphere dominated by H^-. Here we assume that the acoustic heating outside the magnetic field is relatively small which in view of the detection of considerable short period acoustic wave power (periods down to 30 s) by Endler and Deubner (1983) as well as by Deubner (1976, 1985) could be wrong. We do not use the empirical models of Vernazza et al. (1981) because their cell interior model A is based on observations of 5 arcsec resolution which in our view still includes contributions of emission from flux tubes.

At the height of optical depth unity in the outside medium we assume that our three types of magnetic tube have a field strength of $B = 1500$ G and a radius of 53 km. To permit the simplifying assumption that the mean monochromatic intensity J_ν in the H^- continuum is constant as function of height we actually start our calculation 300 km higher at the level where the external optical depth is $1\ 10^{-2}$. Here the tube radius has increased to 95 km and the field strength decreased to $B = 460$ G. As the area of the outside medium is much larger than the tube cross section it is clear that the mean intensity J_ν in the tube is dominated by the outside medium. Therefore, in radiative equilibrium the temperature inside the static tube must be equal to the temperature outside the tube.

Using this property it is easy to compute pressure, density and radius as function of height assuming horizontal pressure balance. The resulting tube we call an *exponential tube*. Rapid spreading of the flux tube cannot go on forever, especially for a tube located in the network region at a supergranulation boundary. Here the spreading tube soon collides with neighbouring tubes. For our second *linear tube* model we thus assume that at the height of 500 km the exponential spreading stops and the tube spreads only linearly thereafter. Our third tube model is the *constant cross section tube*. This model might represent an active region where there are so many emerging flux tubes that there is no room for spreading. As a constant cross section drops out of the hydrodynamic equations, a wave computation using the latter tube actually represents a plane wave calculation, but in an atmosphere with the much reduced gas pressure appropriate within the tube. In the cases where the magnetic field does not spread exponentially we assume additional external magnetic forces to generate the specified tube geometries. This does not affect the internal gas pressure (see Herbold et al., 1985). The shape and the height dependence of the physical variables obtained for these initial pure H^- radiative equilibrium flux tube models are shown in Fig. 1.

2.2. Acoustic wave computation

Acoustic waves of different energy and period were introduced into the flux tubes by moving a piston at the lowermost height point. The wave propagation was computed solving the time-dependent continuity, Euler and energy equations in a Lagrangian frame using the modified characteristics method described by Ulmschneider et al. (1977, 1978) and Herbold et al. (1985). For the energy equation the radiative transfer equations for Ca II K or Mg II k lines and the statistical rate equations for these elements were solved simultaneously as described below. In addition non-LTE non-grey H^- emission was treated following Schmitz et al. (1985). To increase the speed of convergence in our hydrodynamic code we extrapolated the values at the new time step using two previous time steps as described by Ulmschneider (1986a).

2.3. Merging of shocks

When an acoustic wave calculation along an extended flux tube is started it is usually found that the first shock after moving into an undisturbed atmosphere generates a vigorous outflow. After transmission of this shock through the top boundary of the tube, one then finds that the atmosphere contracts and that the second shock will not move very rapidly. In this case a third shock usually overtakes the second one, leading to the merging of the two

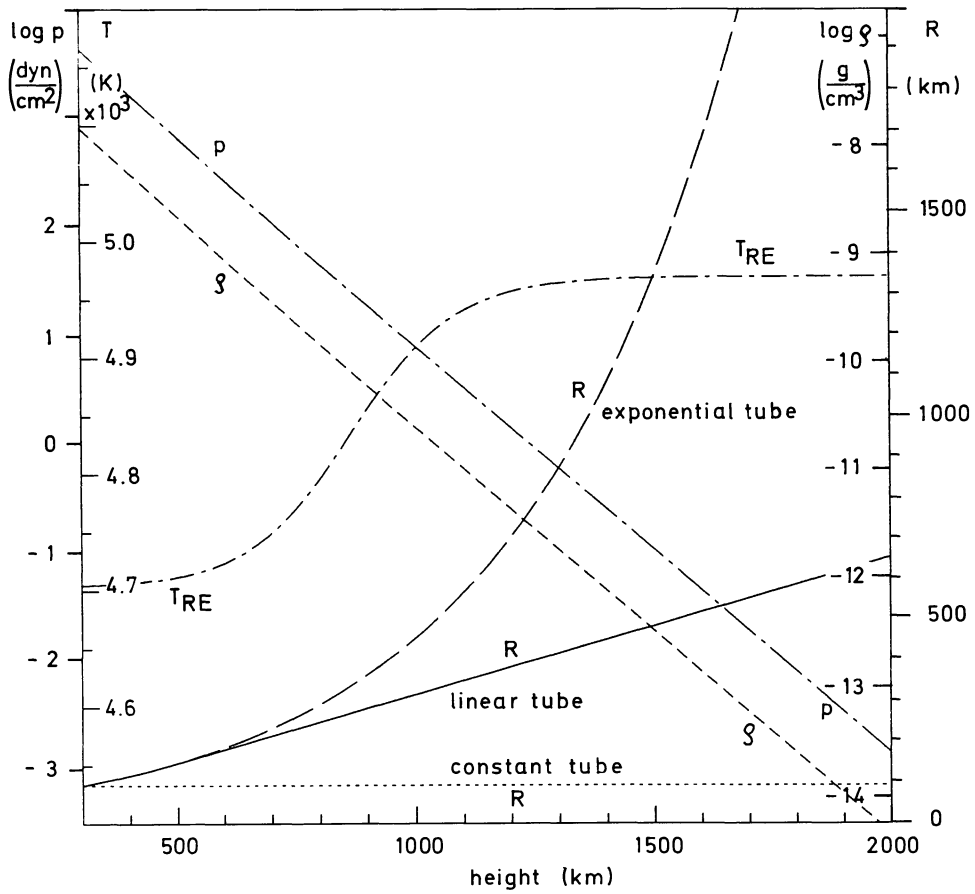

Fig. 1. Temperature T, gas pressure p (dyn cm^{-2}), density ϱ (g cm^{-3}) and radius R for our constant, linear and exponential initial flux tube models. For the constant and linear tubes external magnetic forces are assumed to generate the specified tube geometries

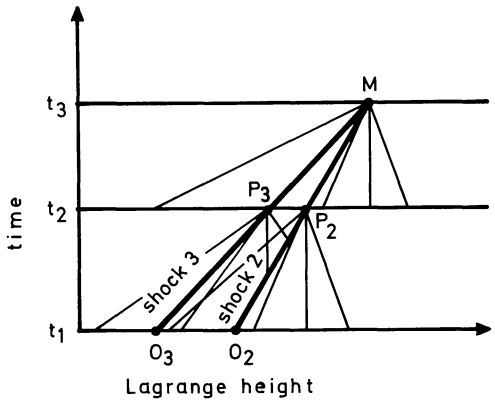

Fig. 2. Characteristics for overtaking shocks

shocks. We have modified our code to allow for shocks of small and moderate strength to merge. Figure 2 shows the characteristics field when shock 3 overtakes shock 2. The physical state at the shock points P_2 and P_3 at time t_2 can be computed as discussed by Ulmschneider et al. (1977) when the state at P_2 is computed before the state at P_3. The only difference is that for the computation of shock 3 information from shock 2 is used by interpolating along the shock path $O_2 P_2$. The position and the physical state of the merging point M is found by extrapolating the shock paths and iterating the time t_3. Here the four indicated characteristics are used.

2.4. Calcium and magnesium line radiation treatment

For the treatment of the Ca II K and Mg II k line emissions we have used the core-saturation method described by Kalkofen and Ulmschneider (1984). We have selected 29 logarithmically spaced wavelength points $\Delta\lambda_j$ to cover each line and have used two angle points. If in this two beam approximation a given monochromatic optical distance $\Delta\tau_{i,j}$ between adjacent spatial grid points, x_i, x_{i+1} was found larger than the fixed limit $\Delta\tau_\gamma$ (for which values between 0.3 and 1.0 were taken), then this frequency was assumed to belong to the line core, otherwise to the line wing. The maximum wavelength offsets from line center, $\Delta\lambda_1$ and $\Delta\lambda_{29}$ were selected such that at the lowest height point we just had a core contribution for these wavelengths.

Taking the horizontal radiative transfer across the tube wall into account is straightforward in principle, although complicated in practice, since an elaborate code is necessary. It is also quite expensive since a sufficiently large number of rays is needed in order to treat the transfer properly in the flaring flux tube (cf. Kalkofen et al., 1986). For the treatment of the line radiation we therefore assume plane-parallel geometry. To justify this assumption, Table 1 shows for the linear tube that the optical distance, $\Delta\tau_H$, horizontally across the tube is larger than the optical depth, $\tau_{i,j}$, from the stellar surface. In addition, photon escape from the atmosphere is enhanced by the outward traveling wave, since the emissivity is strongly peaked in the Doppler-shifted post-shock regions thus reducing the monochromatic optical distance to the outside atmosphere without significantly affecting optical path

Table 1. Monochromatic optical depths $\tau_{i,j}$ at height x_i, compared with the optical distances $\Delta\tau_H$ across the tube at the same height for the linear flux tube model. $\Delta\lambda_j$ are the wavelength differences from line center of the core-wing separation at which the optical distances are given. r_i is the tube radius at height x_i

x_i (km)	r_i (km)	$\Delta\lambda_j$ (mA)	$\tau_{i,j}$	$\Delta\tau_H$
330	102	49.6	11.0	22.7
600	185	13.9	11.4	39.9
900	284	5.04	11.9	60.9
1200	386	3.91	12.2	85.9
1500	487	3.03	6.7	59.3
1800	589	0	10.0	118.

lengths across the tube. Thus, cooling takes place predominantly in the vertical direction. At low heights where $\Delta\tau_H$ becomes comparable to $\tau_{i,j}$ the line radiation is an unimportant part of the total radiative energy flux and can be neglected compared to H^-. For the exponential tube with its larger radius the plane-parallel approximation is even better, while for the constant tube the plane-parallel approximation is poor, if the small photospheric tube radius is adopted.

Mg II line emission was computed assuming an atomic model with two bound levels. Line scattering was calculated under the assumption of complete redistribution. The source function in the two level approximation can then be written (Mihalas, 1970, p. 335; Kalkofen and Ulmschneider, 1984)

$$S_{12}=\frac{\int \varphi_\nu J_\nu \, d\nu + \varepsilon B_{\nu 12}}{\pi_E+\varepsilon}, \tag{1}$$

where the integration is performed only over the wings of the line. $B_{\nu 12}$ is the Planck function and π_E is the escape probability with

$$\pi_E=\int \varphi_\nu \, d\nu, \tag{2}$$

where again the integration is only over the line wings. The photon destruction probability ε is given by

$$\varepsilon=\frac{n_e \Omega_{21}}{A_{21}}\left(1-\exp\left(-\frac{h\nu_{12}}{kT}\right)\right), \tag{3}$$

where n_e is the electron density, T the temperature, ν_{12} the frequency of the line center, Ω_{21} the collisional, and A_{21} the Einstein coefficient for spontaneous emission, h is Planck's and k Boltzmann's constant. φ_ν is the Voigt profile with the damping parameter a computed as by Kalkofen and Ulmschneider. The relevant atomic data for our line calculations are summarized in Table 1 of Kalkofen et al. (1984). The net radiative cooling rate in a two level approximation can then be written

$$\Phi_R = h\nu_{12} n_1 B_{12} \varepsilon \frac{B_{\nu 12}-S_{12}}{1+c^2 S_{12}/(2h\nu_{12}^3)}, \tag{4}$$

where n_1 is the number density of the ground state and B_{12} the Einstein absorption coefficient. In the hydrodynamic calculation where the entropy per gram, S, is used as a thermodynamic variable we have (Ulmschneider et al., 1977, 1978) if Φ_R is the combined H^- and metal line cooling rate

$$D=\left.\frac{dS}{dt}\right|_{Rad} = -\frac{\Phi_R}{\varrho T}, \tag{5}$$

where ϱ is the density.

In the derivation of Eq. (4) the statistical rate equation was used. A more realistic treatment would require the simultaneous solution of the time dependent particle conservation equations (cf. Ulmschneider and Muchmore, 1986). Our present approximation assumes that the collisional excitation and radiative recombination rates are very fast compared to the wave period. Table 2 shows relevant values of collisional excitation times $t_{c12}=(n_e \Omega_{12})^{-1}$. The recombination times $t_{r21}=(n_e A_{21})^{-1}$ (not shown in Table 2) are very short. It is seen that in front of the shocks and in the cool parts of the wave time-dependent excitation effects should be considered. For our present work however only the strongly emitting wave crests and post shock regions are of importance where t_{c12} is very small. Here the usage of the statistical equations is permissible.

The electron population is assumed to arise from two components, the first being single ionization of metals for which the electron number density $n_e = 1\ 10^{-4} n_H$, where n_H is the total hydrogen number density. The second component is due to the hydrogen ionization which was computed in LTE. In the middle and upper chromosphere the hydrogen ionization, which is only very crudely evaluated using LTE, strongly affects the computation of the electron density. As n_e directly enters the Ca II or Mg II radiation treatment (cf. Eqs. 3 and 4) the chromospheric

Table 2. Collisional excitation times t_{c12}, collisional ionization times t_{ci12}, t_{ci23} and radiative recombination times t_{R21}, t_{R32} for Mg and the acoustic wave in the linear tube of Fig. 5 as function of height a, temperature T and electron density n_e. The values at 890 and 1280 km height are for post and pre-shock states

a (km)	T (K)	n_e (cm^{-3})	t_{c12} (s)	t_{ci12} (s)	t_{ci23} (s)	t_{R21} (s)	t_{R32} (s)
570	5610	7.0E11	1.9E-2	3.7E2	6.5E9	3.8E0	9.9E-1
800	3680	2.7E10	6.0E1	4.8E7	2.6E18	1.1E2	1.8E1
890	7530	5.4E12	2.4E-4	7.4E-1	2.6E5	1.7E-1	1.7E-1
890	4250	2.0E9	1.2E2	2.4E7	5.8E16	1.6E3	2.7E2
1280	7530	1.0E12	1.2E-3	3.8E0	1.4E6	9.1E-1	8.7E-1
1280	3910	1.4E8	5.0E3	2.1E9	2.9E19	2.2E4	3.6E3
1380	9990	2.6E10	9.3E-3	7.5E0	1.6E5	1.3E1	4.4E1

radiation loss is likewise strongly affected. Furthermore, Kneer (1980) has shown that there are important time-dependent effects for the hydrogen ionization balance. As a detailed computation of these effects must await a consistent hydrogen treatment and cannot be undertaken within the scope of the present paper, we unfortunately are not able to estimate the severity of the error we are making.

For the ionization of Mg I to Mg II and of Mg II to Mg III Table 2 shows values of collisional ionization and radiative recombination times defined analogously to the excitation times above. It is seen that in the important post shock and wave crest emission regions the radiative recombination times are fast compared to the wave period permitting the neglect of time-independent effects. The Mg ionization was computed in LTE. Since Mg occurs mainly as Mg II, departures from LTE are probably not very important. Similar assumptions were made for Ca.

In the core-saturation method of Kalkofen and Ulmschneider (1984) the source function is found by a lambda iteration, requiring about 20 iterations for convergence if one starts from scratch. Convergence is faster in our computations because the source function from the previous time step serves as an excellent initial estimate for the new time step. In addition, the source function iteration is embedded within the iterations for the hydrodynamical variables and the radiative transfer so that in most instances a still better starting estimate is available. Thus only about 3 lambda iterations were generally necessary for $|\Delta D| < 10^{-2}|D|_{\max}$ at every height.

For the solution of the energy equation the total chromospheric radiation loss is required. In a typical calculation we only evaluate the H^- continuum and e.g. the Mg II k line losses. The total chromospheric emission as determined empirically by Vernazza et al. (1981) involves with the Mg II h and k and the Ca II H, K and IRT lines seven relatively strong lines in addition to the H^- and hydrogen contributions. The hydrogen contribution in the chromosphere comes mainly from the Hα line and the Balmer continuum. However, Vernazza et al. have shown that these two, one being a cooling and the other a heating mechanism, cancel energetically such that the net hydrogen contribution to the chromospheric emission is small. To take into account all the neglected contributions of the principal chromospheric lines and continua we have scaled the Mg II k line results as discussed below.

3. Comparison with the computations of Vernazza, Avrett and Loeser

To enable a time-dependent treatment of the Mg II or Ca II line radiation many simplifying assumptions were made in our work: First, we took only a very crude atomic model with two bound levels for the Mg II or Ca II ions. Second, we have treated the hydrogen ionization in LTE as opposed to more realistic treatments where departures from LTE are taken into account (e.g. Vernazza et al., 1981). Third, assuming complete redistribution we have neglected the partially coherent scattering in the line wings. Coherent scattering, by preventing photons from migrating in frequency to the line wings, leads to a more rapid saturation of the source function to the Planck function and thus according to Eq. (4) to less emission. The assumption of complete redistribution thus generates an overestimate of the line emission. Fourth, we have computed the ionization of Mg I to Mg II and of Mg II to Mg III in LTE. As discussed above, this is probably not so bad since the bulk of Mg is in the Mg II state; the same is valid for Ca. Finally, the core-saturation method has ambiguities associated with the free choice of the parameter $\Delta\tau_\gamma$ to define the core-wing separation as discussed above.

In view of all these limitations, it is useful to compare our method of computing line emission with more elaborate calculations found in the literature. Using their distributions of temperature, electron density and total hydrogen number density of the emitting elements we have recomputed the Ca II K and Mg II k line emissions of model C of Vernazza et al. (1981) using our method. Note that we did not use our LTE treatment of the H ionization here. A comparison of the net radiative cooling rates is shown in Fig. 3. As expected it is seen that our method overestimates their Ca II and Mg II line emissions especially at low heights where the energetically significant radiative exchange occurs in the wings (cf. Table 1) and where the complete redistribution assumption is especially poor. That the assumption of complete redistribution increases the emission rate at low heights by up to a factor of ten as compared to the assumption of partial redistribution has been confirmed by Avrett and Loeser (1966) for their models.

To investigate the intrinsic uncertainty of the core-saturation method we have computed two cases with $\Delta\tau_\gamma = 0.3$ and 1.0. In addition because the height steps in the Vernazza et al. model are much larger than those in our hydrodynamic computations we have increased the number of height points in their model by a factor of three. It is seen in Fig. 3 that the choice of $\Delta\tau_\gamma$ does not affect the emission rate very much. Figure 3 also shows cases labeled LTE in which the line emission was computed using the

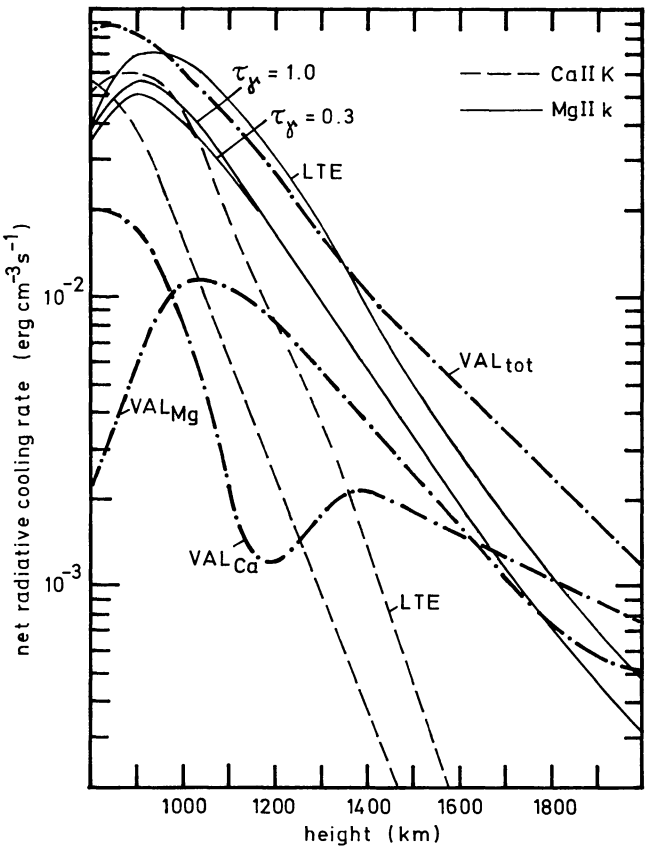

Fig. 3. Comparison of our computed Ca II K and Mg II k line radiative cooling rates (thin) with values (thick, labelled VAL) given by Vernazza et al. (1981) for their model C

temperature and gas pressure distribution of the Vernazza et al. model and computing the H ionization in LTE. This is the procedure which we employ in our time-dependent wave calculations as discussed below in Sect. 4. It is seen that the neglect of departures from LTE in hydrogen increases the emission by a factor of about 1.6 for Mg and 3 for Ca which is due to the fact that in LTE the electron density is increased.

In all of the above cases the Ca II and Mg II line computations exceeded the results of Vernazza et al. For a more realistic emission we would be led to scale down the rates obtained from our computations. On the other hand, for the solution of the energy equation we need the total chromospheric radiation loss rather than an individual line contribution. In view of the seven main emission lines as discussed above, this could be achieved by scaling up an individual line contribution. As our Mg II line emission rates together with the H^- results are roughly equal to the total cooling rates of Vernazza et al. we dispense with any scaling and take our overestimated radiation loss for this one line to simulate the total chromospheric emission. To extend this assumption to nonstatic situations is a further approximation, the validity of which can only be evaluated by more elaborate computations.

4. Results and discussion

4.1. Strong dependence on the tube geometry

Figures 4 to 6 show snapshots of acoustic waves propagating along our three different flux tube models: the *constant tube*, the *linear tube* and the *exponential tube*. The computations were all made with the same period 45 s and the same initial energy flux $F_M = 2.5\ 10^7\ \mathrm{erg\,cm^{-2}\,s^{-1}}$ using $\Delta\tau_y = 0.3$. The waves are shown at similar phases and are plotted on the same scale. Comparing the three waves e. g. at the compression region at 550 km height we see that the wave in the constant tube has much larger temperature and velocity amplitudes than the waves in the linear and exponential tubes. The two latter waves have nearly the same amplitude at this point since both tubes retain the same cross-section up to 500 km height. At the height of 1300 km the amplitudes of all three waves differ greatly from one another. The behaviour at both heights is consistent with what one expects from energy conservation in tubes which spread at different rates. The larger the tube cross section becomes, the greater is the area over which the wave energy flux is distributed and the smaller are the wave amplitudes.

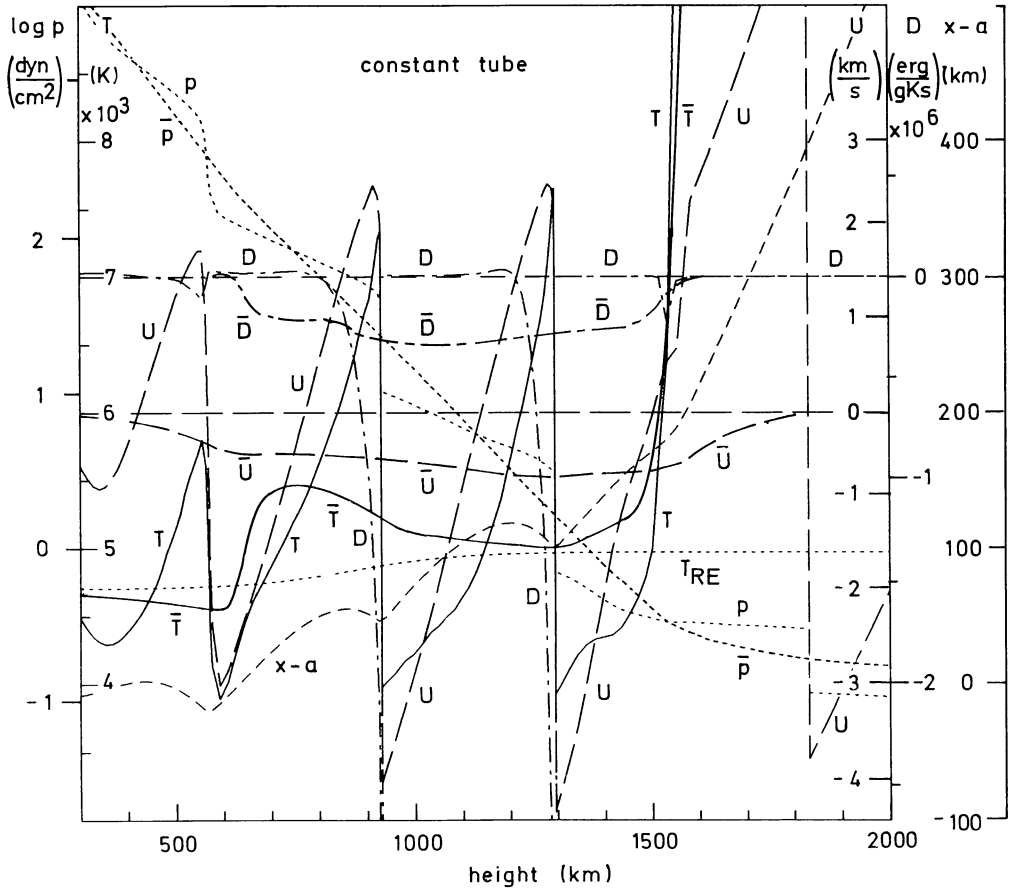

Fig. 4. Temperature T, velocity u, pressure p and damping function D together with the time-averaged values T, $\bar{u}$, $\bar{D}$ for an acoustic wave in a tube of *constant cross section*. x-a is the height displacement of the mass elements at (Eulerian) height x which at time zero were at the (Lagrange) height a. T_{RE} indicates initial radiative equilibrium temperature. The wave has a period of 45 s and an initial flux $2.5\ 10^7\ \mathrm{erg\,cm^{-2}\,s^{-1}}$ and is shown at the time 1772 s

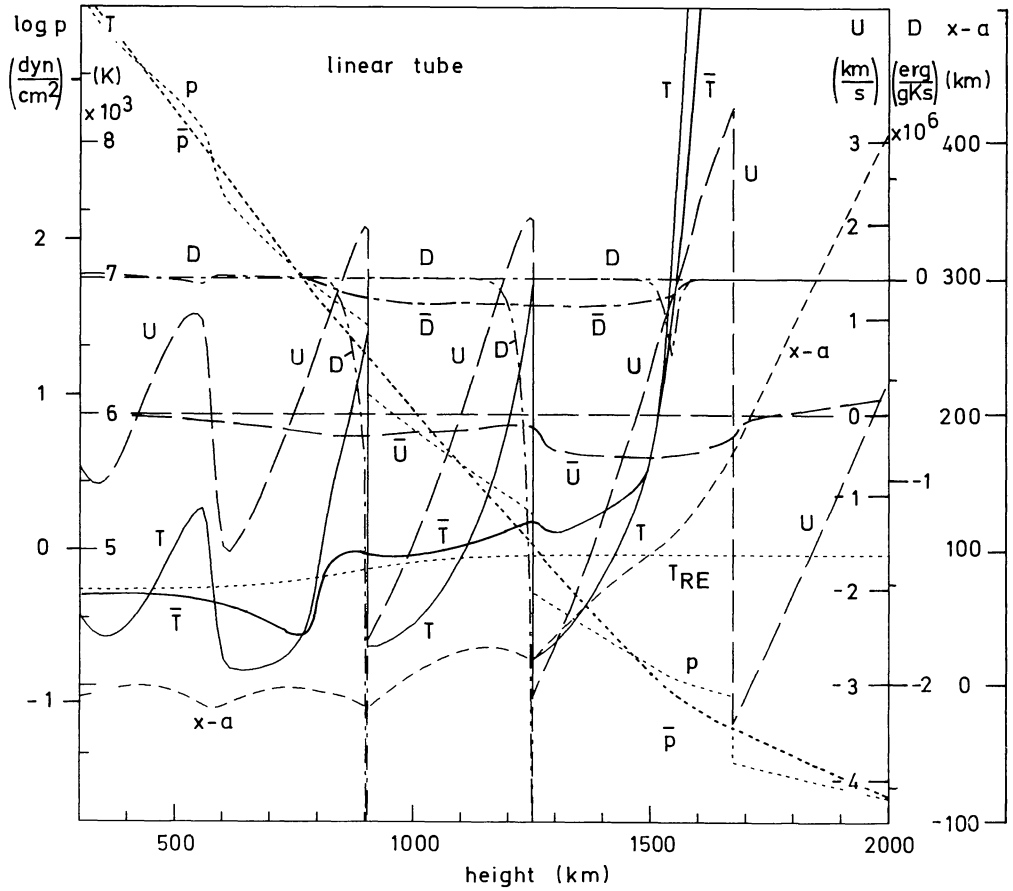

Fig. 5. Same as Fig. 4 however for a *linear tube* at the time 1772 s

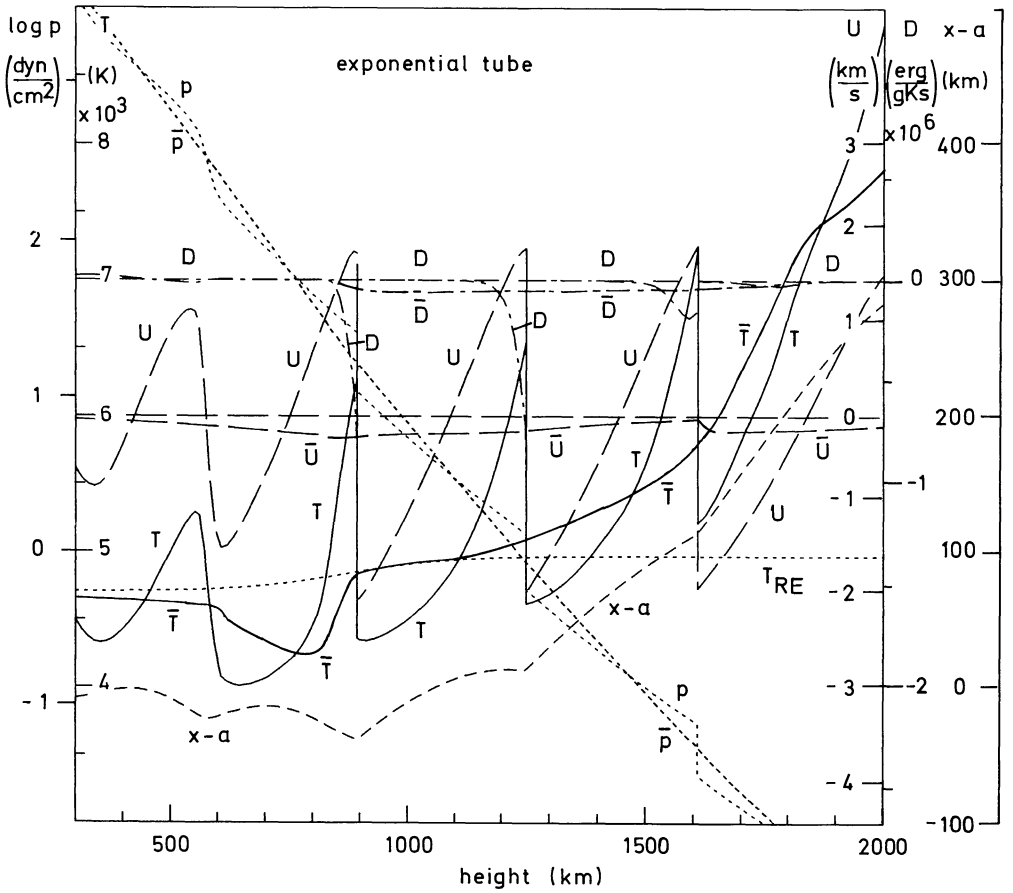

Fig. 6. Same as Fig. 4 however for an *exponential tube* at the time 3752 s

4.2. Formation of a rapid temperature rise

Figures 4 to 6 show that at Euler heights on the order of 1500 to 2300 km transition layer-like steep temperature gradients develop. The wave in the constant tube shows a rapid temperature rise at about 1500 km. The wave in the linear tube has a steep temperature rise at about 1600 km and the wave in the exponential tube at about 2200 km height. It is seen that the position of the rapid temperature rise depends strongly on the tube geometry, and occurs at greater height the more rapidly the tube spreads. All our present wave calculations produce steep temperature rises. This is similar to what we found in wave calculations with H^- as the only emitter (Schmitz et al., 1985) where we also obtained transition layer-like rapid temperature rises in every case. The appearance of steep temperature rises in our present calculations can be understood as follows: At great heights, depending on pressure and temperature, Mg II is ionized to Mg III. As H^- occurs only at low heights and thus is negligible, the Mg II ionization constitutes the destruction of the only remaining emitter. The heat deposited by shock dissipation can therefore no longer be balanced by radiative cooling, thus leading to a rapid rise of the mean temperature. The physical reason for the generation of a steep temperature rise in our calculations, the destruction of the remaining important emitter and unbalanced shock heating is the same one that we found in our H^- computations.

Although the discussion of the basic physics of the generation of the observed transition layer must await work which includes the treatment of hydrogen, it is interesting to speculate about what the inclusion of hydrogen might do to our rapid temperature rises. The most serious defect in our models is that at the point where the rapid temperature rise occurs Lyα cooling will be important. This situation is similar to our pure H^- models (Schmitz et al., 1985) were the steep temperature rise caused by the ionization of H^-, occurs at the point where Mg II line emission becomes important. Comparison with our present models shows that the inclusion of the Mg II line emission extends the chromosphere and thus increases the height of the rapid temperature rise. This comparison suggests that similar to the inclusion of Mg II, the inclusion of H will lead to a chromosphere extended even further. When the ionization of H removes an efficient cooling mechanism from the gas, a rapid temperature rise should be generated.

4.3. Generation of mass motion

Energy conservation requires that the wave energy dissipated by shocks and converted into thermal energy must either be radiated away or lead to adiabatic expansion. Mass motion then occurs if at great height the main remaining cooling mechanism is destroyed. As the density in all three tubes is the same function of height it is seen that the lower the height of the rapid temperature rise is, the denser is the region where mass motion begins and the larger is the mass flux generated. Mass motion thus depends strongly on the tube geometry. In Figs. 4 to 6 it is seen that the displacement of the eulerian height x from lagrangian height a begins to become significant where the rapid temperature rises form. Large mass motion is produced in the constant tube; comparatively little in the exponential tube. At low height where shock dissipation is balanced by radiative cooling the mean value of $x-a$ becomes constant after sufficient time and a dynamical steady state with negligible mass flux develops. At great height the mass motion is due to the adjustment of the atmosphere to the much larger scale height generated by the rapid temperature rise. For lack of (radiative or thermal conductive) cooling this rise steadily increases in steepness and thus the mass motion does not reach a steady state in our calculations. However, Cuntz et al. (1986) have shown that in their Arcturus model with monochromatic short period waves (as in our present case), the inclusion of a cooling mechanism always leads to a dynamical steady state without mass loss. This suggests that all the mass motions generated in Figs. 4 to 8 are transient in nature. They would cease eventually if an adequate cooling mechanism were included.

4.4. Radiation loss produced by the waves

Figures 4 to 6 show that large temperature variations in the waves, particularly behind shocks, produce large variations in the radiative emission. In addition the variation of the temperature amplitudes due to the different tube geometries strongly affects the radiative cooling rate. The radiative cooling rate Φ_R is given in our figures in terms of the radiative damping function D of Eq. (5). In Fig. 4 the values of D behind the shocks at the heights 930 and 1290 km are $-1.5\ 10^7$ and $-9.2\ 10^6$ erg $s^{-1}\,g^{-1}\,K^{-1}$, respectively; in Fig. 5 the corresponding values are $-3.2\ 10^6$ and $-2.9\ 10^6$ at 900 and 1260 km. For the maximum of $|D|$ one has about $1.7\ 10^7$, $4\ 10^6$ and $1\ 10^6$ erg $s^{-1}\,g^{-1}\,K^{-1}$ for the constant, linear, and exponential tube respectively. While for the time-averaged $\bar{D}$ one finds $3.5\ 10^5$, $1.2\ 10^5$ and $6\ 10^4$ erg $s^{-1}\,g^{-1}\,K^{-1}$ for the constant, linear and exponential tubes respectively. There is roughly a factor of four (three) difference in the maximum (average) radiative cooling rate per gram between the three tubes. This strong temperature dependence of the Mg II k line emission is understood from the fact that after Eqs. (3) and (4) both ε (as function of n_e) and $B_{\nu 12}$ depend strongly on temperature. The source function S_{12} is small and varies only slowly with height. It is seen that the emission is concentrated in intensely radiating layers behind the shock. In front of the shock, due to the small electron density, ε is many orders of magnitude smaller than behind the shock, resulting in negligible absorption. At great height due to the ionization of Mg II into Mg III the radiative damping vanishes. Figures 4 and 5 show that due to the strong radiation damping the mean temperature $\bar{T}$ sometimes has a decreasing behaviour with height which one would not expect on basis of the models of Vernazza et al. (1981). As the strong postshock temperature regions dominate the emergent emission spectrum from our models (work in preparation) we found that the decreasing average temperature does not become apparent in the spectrum.

4.5. Characteristic shape of the shocks and the mean velocity

Strong radiative relaxation behind the shocks leads to characteristic shock wave profiles. Comparing Figs. 4 and 6 it is seen that in cases with strong radiation losses a sharply peaked temperature behind a shock is correlated with a flat velocity profile. This is understood from the momentum and energy equations. Strong radiative cooling behind the shock primarily affects the kinetic temperature. Through the strongly decreasing kinetic motion of the atoms and ions the pressure is decreased relative to the adiabatic case as can be seen by comparing Figs. 4 and 6 behind the shocks. In this process the density of the gas is less strongly affected. From the momentum equation it is then seen that a decreased pressure amplitude results in a reduced velocity amplitude.

Another interesting feature of Figs. 4 to 6 is that the time averaged velocity $\bar{u}$ in the region below the rapid temperature rise is negative. This is understood from our eulerian averaging procedure. $\bar{u}$ was obtained by averaging the velocity at a fixed

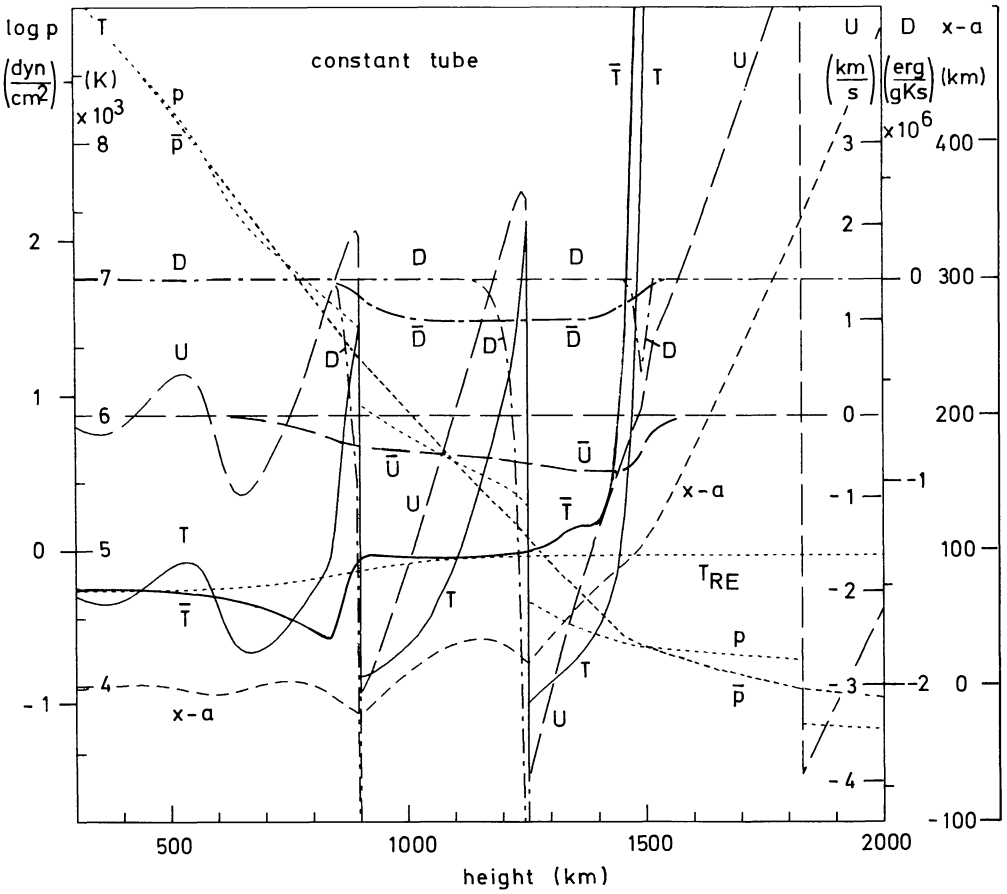

Fig. 7. Same as Fig. 4 however for an initial flux of 1.5 10^6 erg $cm^{-2}\,s^{-1}$ at the time 1772 s

eulerian height. In our calculation after an initial switch-on effect a dynamical steady state is reached and no mass flow is found. Thus the time-average of the mass flux ϱu must be zero. In this averaging of ϱu the positive velocity amplitude behind the shock is weighted by a larger ϱ and the negative velocity amplitude in front of the shock by a small ϱ. When $\overline{\varrho u}$ is zero then $\bar{u}$ must be negative.

4.6. *Influence of the wave energy flux*

In Fig. 7 a wave calculation in the *constant tube* with the same wave period as in Fig. 6 but with a reduced energy flux $F_M = 1.5\ 10^6$ erg $cm^{-2}\,s^{-1}$ is shown. The comparison with Fig. 4 shows that the less energetic wave forms a temperature minimum at 830 km height instead of 610 km for the more energetic wave. This shows that decreasing the wave energy leads to shock formation at greater heights, an effect which has also been established by our previous work (Ulmschneider et al., 1977, 1978; Schmitz et al., 1985). When shocks are formed at low heights then shock heating leads to increased mean temperatures and strong radiative damping. Thus the wave with high flux loses much of its energy at low heights. Comparison of Figs. 4 and 7 shows that at 1290 km height both waves have essentially the same energy, notwithstanding that the initial fluxes differ by a factor of 17. At these greater heights, the radiation losses become small and there is now enough heating to raise the chromospheric temperature sharply, triggering the onset of a rapid temperature rise in both cases at the height of 1500 km. Computations with other initial fluxes confirmed that for a given wave period the height of the onset of the transition layer was nearly independent of the initial wave energy. For the *linear tube* we found the same behaviour, however, the transition layer occurred at 1600 km.

4.7 *Differences due to variation of the wave period*

Figure 8 shows a wave calculation in the *constant tube* with an initial wave flux of 6 10^6 erg $cm^{-2}\,s^{-1}$ and with the period of 90 s. It is seen that the 90 s wave produces a rapid temperature rise at 1300 km height (1500 km for the *linear tube*), which is much lower than that for the 45 s wave. This is due to the fact that waves of longer period generate stronger shocks (see e.g. Schmitz et al., 1985). In addition long period waves have much smaller radiation damping and transmit more energy into higher layers. Stronger shocks produce larger temperature spikes at low heights which help to ionize Mg II behind the shock. The destruction of the main radiative emitter thus triggers the formation of a rapid temperature rise at lower height. As discussed above this has the consequence that long period waves produce more mass motion. As the dissipation of the wave energy occurs only at the shock front and as the amount of shock heating for similar wave amplitudes increases with the number of shocks per unit time, it is seen that long period waves produce much less chromospheric heating, a fact already known from analytical arguments (Ulmschneider, 1971) and from previous numerical models (Ulmschneider et al., 1977). We thus find that long period waves

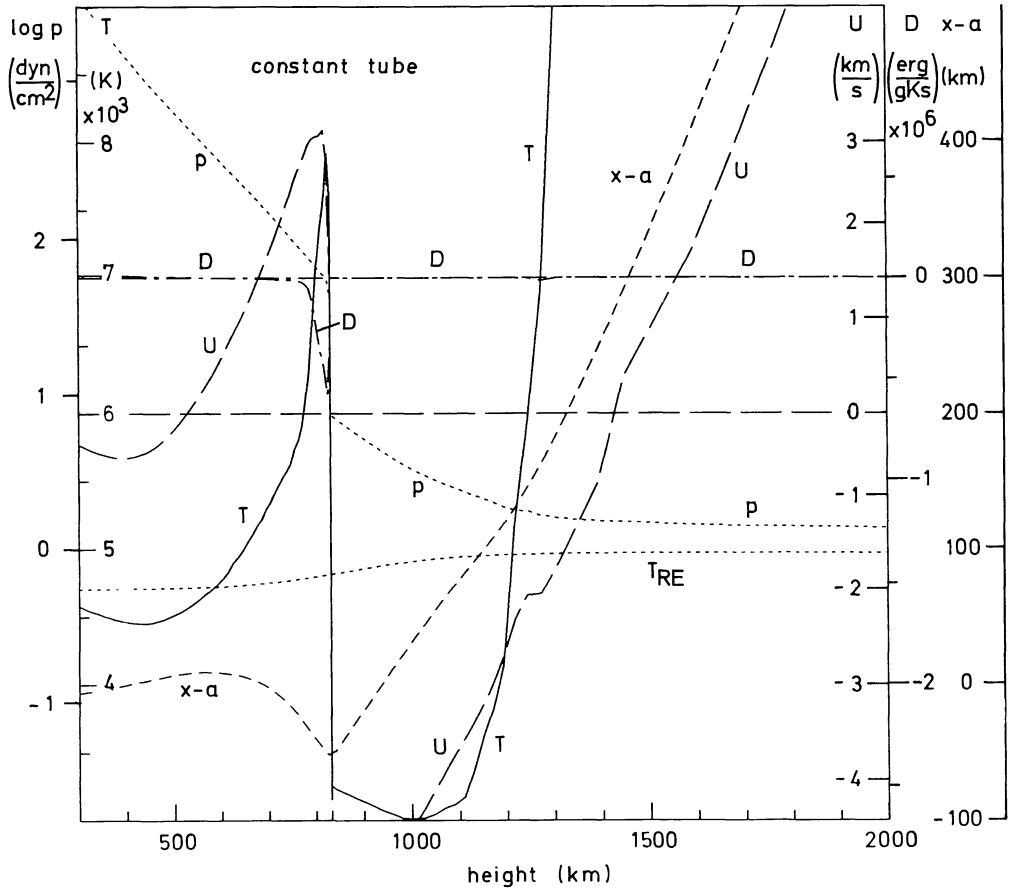

Fig. 8. Same as Fig. 4 however for a period of 90 s and an initial flux of 6.0 10^6 erg $cm^{-2} s^{-1}$ at the time 1467 s

produce rapid temperature rises at lower heights, but put more energy into mass motion and less into chromospheric heating. Computations of 90 s waves with other initial fluxes showed that the height of the rapid temperature rise was again largely independent of the initial wave flux.

5. Conclusions

We have shown that the tube geometry, by spreading wave energy over the cross-sectional area, greatly affects the wave amplitudes. Large wave amplitudes are found in tubes of *constant cross-section* which are relevant for the crowded conditions in active regions. *Linearly expanding tubes* possibly relevant for network regions lead to decreased amplitudes, and *exponentially expanding tubes* relevant for supergranulation cell interiors show small amplitudes at chromospheric heights. In all cases transition layer-like rapid temperature rises eventually developed. In constant tubes these rapid temperature rises developed at low height, in linear tubes at intermediate height and in exponential tubes at great height. The onset of the rapid temperature rise in our calculations is due to the ionization of Mg II and thus to the destruction of the only remaining radiative cooling mechanism. Unbalanced heating quickly increase the temperature and leads to considerable transient mass flows. The gas flows are more massive the deeper the rapid temperature rises form. The conclusions concerning rapid temperature rises are qualitatively the same as those from earlier calculations (Schmitz et al., 1985) which used only H^- as radiative cooling. Comparison of our present models with these pure H^- models suggests that more realistic models which include Lyα should lead to similar rapid temperature rises in more extended chromospheres.

Large temperature amplitudes due to the strong temperature sensitivity of the Mg II emission lead to large radiation losses in the waves. The radiative emission was greatest in the constant cross-section tube, about a factor of four smaller in the linear tube and another factor of four smaller in the exponential tube. As found in earlier work the present computations show that although the low chromosphere is greatly affected by the initial wave energy, the higher chromospheric temperatures are not. This is due to the fact that a more energetic wave forms shocks lower in the atmosphere and at low height loses the wave energy by strongly increased radiative damping. The height of the onset of the rapid temperature rise did not depend much on the initial wave flux. Our computations show that this height is lower with increasing wave period but higher for more rapidly spreading tubes.

Acknowledgements. We thank Drs. E. Avrett and R. Loeser for the computation of solar models assuming complete redistribution, Dr. P. Höflich for helpful discussions and the Sonderforschungsbereich 132 for its generous support.

References

Avrett, E.H., Loeser, R.: 1986 (private communication)
Ayres, T.R.: 1981, *Astron. Astrophys.* **244**, 1064
Basri, G.S., Linsky, J.L.: 1979, *Astrophys. J.* **234**, 1023
Cuntz, M., Hartmann, L., Ulmschneider, P.: 1986, in *Circumstellar Matter*, *Proc. IAU Symp.* **122**, ed. I. Appenzeller, Reidel, Dordrecht (in press)
Deubner, F.-L.: 1976, *Astron. Astrophys.* **51**, 189
Deubner, F.-L.: 1985, *Chromospheric Diagnostics and Modelling*, B. Lites, ed., Sacramento Peak Obs., Sunspot, p. 279
Endler, F., Deubner, F.-L.: 1983, *Astron. Astrophys.* **121**, 291
Herbold, G., Ulmschneider, P., Spruit, H.C., Rosner, R.: 1985, *Astron. Astrophys.* **145**, 157
Kalkofen, W., Rosner, R., Ferrari, A., Massaglia, S.: 1986, *Astrophys. J.* **304**, 519
Kalkofen, W., Ulmschneider, P.: 1984, *Methods in Radiative Transfer*, ed. W. Kalkofen, Univ. Press, Cambridge, p. 131
Kalkofen, W., Ulmschneider, P., Schmitz, F.: 1984, *Astrophys. J.* **287**, 952
Kneer, F.: 1980, *Astron. Astrophys.* **87**, 229
Mihalas, D.: 1970, *Stellar Atmospheres*, Freeman, San Fransisco
Muchmore, D., Ulmschneider, P.: 1985, *Astron. Astrophys.* **142**, 393
Schmitz, F., Ulmschneider, P., Kalkofen, W.: 1985, *Astron. Astrophys.* **148**, 217
Stein, R.F.: 1981, *Astrophys. J.* **246**, 966
Stenflo, J.O.: 1978, *Rep. Prog. Phys.* **75**, 3
Ulmschneider, P.: 1971, *Astron. Astrophys.* **14**, 275
Ulmschneider, P.: 1985, Proc. *Workshop on Theoretical Problems in High Resolution Solar Physics*, ed. H.U. Schmidt, Max-Planck-Institut für Physik und Astrophysik, Munich, p. 150
Ulmschneider, P.: 1986a, *Astron. Astrophys.* **168**, 308
Ulmschneider, P.: 1986b, in *Stellar and Solar Activity*, COSPAR, Proc. Symp. **11**, Toulouse, Adv. Space Res. (in press)
Ulmschneider, P., Kalkofen, W., Nowak, T., Bohn, H.U.: 1977, *Astron. Astrophys.* **54**, 61
Ulmschneider, P., Muchmore, D.: 1986, *Small Magnetic Flux Concentration in the Solar Photosphere*, eds. W. Deinzer, M. Knölker, H.H. Voigt, Abhandl. Akad. Wissensch., Vanderhoeck and Ruprecht, Göttingen
Ulmschneider, P., Schmitz, F., Kalkofen, W., Bohn, H.U.: 1978, *Astron. Astrophys.* **70**, 487
Ulmschneider, P., Stein, R.F.: 1982, *Astron. Astrophys.* **106**, 9
Vernazza, J.E., Avrett, E.H., Loeser, R.: 1981, *Astrophys. J. Suppl.* **45**, 635
Zwaan, C.: 1978, *Solar Phys.* **60**, 213